

WOJCIECH POLITALSKI\*

## NUMERICAL ANALYSIS OF THREE-SPAN SLAB POST-TENSIONED WITH UNBONDED TENDONS AT ULTIMATE

### ANALIZA NUMERYCZNA TRÓJPRZESŁOWEJ PŁYTY SPRĘŻONEJ CIĘGNAMI BEZ PRZYCZEPNOŚCI W STANIE GRANICZNYM NOŚNOŚCI

#### Abstract

The design of multi-span structures post-tensioned with unbonded tendons may differ from the assigned one for reinforced structures or structures post-tensioned with bonded tendons. In some cases Ultimate Limit State can be reached by different loading patterns to which we got used to i.e. load cases which result in maximum values of bending moments in spans and at supports. This behaviour is related to the lack of bond between concrete and strands and the assumption that the force in tendons has a uniform value between anchorages.

*Keywords: design process, stress increase in unbonded tendons, multi-span members*

#### Streszczenie

Projektowanie konstrukcji wieloprześlowych sprężonych cięgnami bez przyczepności może się różnić od tego, które jest wykorzystywane w konstrukcjach żelbetowych bądź sprężonych cięgnami z przyczepnością. W niektórych przypadkach Stan Graniczny Nośności może zostać osiągnięty przez inne schematy obciążenia do których jesteśmy przyzwyczajeni, tj. przypadki obciążeń, w których otrzymujemy maksymalne wartości momentów zginających w przęsłach i nad podporami. To zjawisko jest związane z brakiem przyczepności pomiędzy betonem i zbrojeniem sprężającym oraz założeniem, że siła w cięgnie przyjmuje jednorodną wartość pomiędzy zakotwieniami.

*Słowa kluczowe: projektowanie, przyrost naprężeń w cięgnach, elementy wieloprześlowe*

DOI: 10.4467/2353737XCT.15.169.4344

\* Ph.D. Eng. Wojciech Politalski, Institute of Building Materials and Structures, Faculty of Civil Engineering, Cracow University of Technology.

## 1. Introduction

Codes recommendations [1–3] treat unbonded tendons stress increase in continuous members in a superficial way. The ACI Code design equations for calculating stress increase do not make distinctions between simply supported and continuous members. The opportunity to achieve lower values of stress increase in multi-span members compared to simply supported elements in the case of loading which does not act at all spans simultaneously is disregarded by EC 2. Even though such a possibility is mentioned in Polish Code no detailed provisions are given.

Due to the abovementioned situation, strategies for solving the problem of stress increment in multi-span unbonded members are sought and can be successfully found in theories proposed by various authors [4–7]. The proposed equations assigned for continuous members account for expansions of equations derived firstly for simply supported members. Hence the fact that the loading pattern factor for simply supported beams is equal to 1.

Numerous items of data relating to the testing of simply supported members can be found in literature. Due to the fact that the conducting research on multi-span structures is much more complicated, only a few examples can be found in publications. Numerical analysis based on tests conducted by Burns et al. [8] was carried out. The received results were compared with analytical calculations obtained using various theories regarding the loading pattern factor which were derived by Naaman and Harajli [4–7].

## 2. Experimental test by Burns et al.

Elements Slab A and Slab B tested by Burns et al. [8] were three-span slabs. The length of each span was the same and was equal to 6.1 m. The cross-section height was 140 mm. In fact members were half-scale models. In order to obtain proper scaling for self-weight, live-loading and prestress, the span length, cross-section height and effective depth were reduced to 50% and the cross-section width and self-weight were increased up to 200%. Slab A and Slab B differ in their ordinary and prestressing reinforcement ratios. They were designed in such a way that the sum  $q_0$  of the ordinary reinforcement index  $q_s$  and the prestressing reinforcement index  $q_e$  for each member was the same. The indices are defined as follows:  $q_s = (\rho_s f_y) / f'_c$  and  $q_e = (\rho_p f_{pe}) / f'_c$ . Geometric and materials' characteristics are presented in Table 1. View and cross-sections are shown in Fig. 1. The lengths of reinforcing bars in spans and at supports are not given – the only information provided for this is that they were too short. The main crack which determined the location of the crucial cross-section at ultimate was localised near to the end of ordinary reinforcement.

Utilised loading patterns are gathered in Table 2. Combinations 108–110 and 208–210 led to the slabs' failure. It can be observed that in almost all of over mentioned combinations, except full loading in one or two spans there is acting percentage of loading in other spans.

Table 1

**Geometry and materials' characteristics of half-scale members tested by Burns et al.**

Members' name	Span length	Cross-section's dimensions [mm]				Concrete	Prestressing reinforcement					Ordinary reinforcement				Steel
	lefft	h	dp	ds	b	$f_c$	wires	$A_p$	$q_c$	$f_{py}$	$f_{pu}$	bars	$A_{s1}$	$f_y$	$q_s$	$q_0$
	[m]					[MPa]	[n × Ø]	[mm <sup>2</sup> ]	[-]	[MPa]	[MPa]	[n × Ø]	[mm <sup>2</sup> ]	[MPa]	[-]	[-]
Slab A	3 × 3.05	70	57	57	1397	32.4	4 × φ6.3	127	0.048	1469	1655	4 #2	127	448	0.022	0.070
Slab B						35.5	3 × φ6.3	95	0.034			7 #2	222		0.035	0.069

**Slab A and Slab B - view**

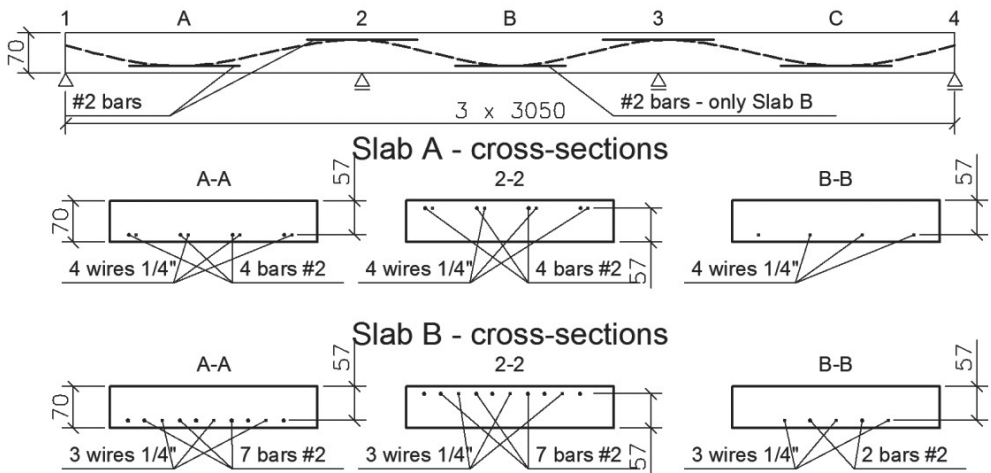


Fig. 1. View and cross-sections of members tested by Burns et al.

Table 2

**Loading patterns of three-span members tested by Burns et al.**

Loading pattern	Slab A – loading [kN/m <sup>2</sup> ]			Loading pattern	Slab B – loading [kN/m <sup>2</sup> ]		
	span A	span B	span C		span A	span B	span C
101	2.4	2.4	2.4	201	1.7	1.7	1.7
102	2.4	0.0	2.4	202	2.4	2.4	2.4
103	0.0	2.4	2.4	203	2.4	2.4	0.0
104	5.0	2.4	5.0	204	4.8	0.0	4.8
105	4.9	4.9	2.4	205	4.8	4.8	4.8
106	5.0	0.0	5.0	206	5.5	5.5	5.5
107	5.5	5.5	5.5	207	5.5	5.5	1.3
108	6.5	1.3	6.5	208	5.7	1.3	5.7
109	7.4	7.4	1.3	209	1.3	6.9	6.9
110	0.0	7.2	0.0	210	1.3	7.6	1.3

### 3. Numerical analysis – assumptions

Numerical analysis was conducted using FEM DIANA [9]. A total Strain Fixed crack model for concrete was used. The tensile stress-strain relationship is described by brittle cracking behaviour (Fig. 2a), the compressive stress-strain relationship is described by a multilinear diagram (Fig. 2b).

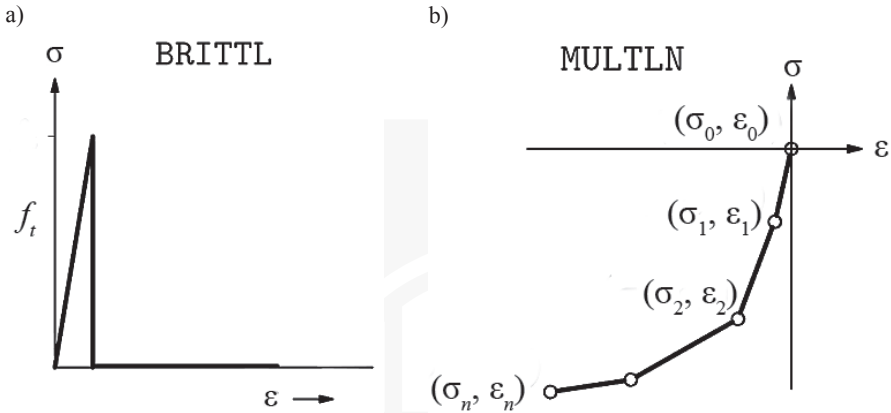


Fig. 2. Total Strain Fixed crack model for concrete a) in tension b) in compression

Initially, the target of the numerical analysis was a comparison of its results with the findings of experimental tests conducted by Burns et al. This intention was relinquished due to the following reasons:

- a limited amount of data relating to materials' properties and a lack of information regarding the Young modulus and tensile strength of concrete,
- preliminary failure of structure connected with lengths of reinforcing bars at supports that were too short,
- member failure was caused by not “basic” load patterns i.e. combination where except maximum loadings in spans partial loading in other spans was also acting.

Due to these facts the following assumptions were made:

- the concrete Young modulus of elasticity was calculated according to equation (1):

$$E_{ci} = 4700 \cdot \sqrt{f'_c} \quad (1)$$

- the brittle cracking models of concrete in tension shown in Fig. 3a were used,
- Hognestad compressive behaviour of concrete calculated in accordance with equation (2), with values given in Table 3 as shown in figure 3b were used:

$$\sigma = f'_c \cdot \left[ 2 \frac{\varepsilon}{\varepsilon_0} - \left( \frac{\varepsilon}{\varepsilon_0} \right)^2 \right] \quad 0 \leq \varepsilon \leq \varepsilon_0; \quad \sigma = f'_c \cdot \left[ 1 - 0.15 \cdot \left( \frac{\varepsilon - \varepsilon_0}{\varepsilon_{cu} - \varepsilon_0} \right) \right] \quad \varepsilon_0 \leq \varepsilon \leq \varepsilon_{cu} \quad (2)$$

Stress-strain relationship for concrete in compression

Multilinear diagram values of $\sigma(\epsilon)$ relationship for concrete in compression – Slab A													
Strain [%]	0	0.24	0.48	0.73	0.97	1.21	1.45	1.70	1.94	2.18	2.42	3.00	3.01
Stress [MPa]	0	6.2	11.7	16.5	20.7	24.3	27.2	29.5	31.1	32.1	32.4	27.5	0.1
Multilinear diagram values of $\sigma(\epsilon)$ relationship for concrete in compression – Slab B													
Strain [%]	0	0.25	0.51	0.76	1.01	1.27	1.52	1.77	2.03	2.28	2.54	3.00	3.01
Stress [MPa]	0	6.7	12.8	18.1	22.7	26.6	29.8	32.3	34.1	35.1	35.5	30.2	0.1

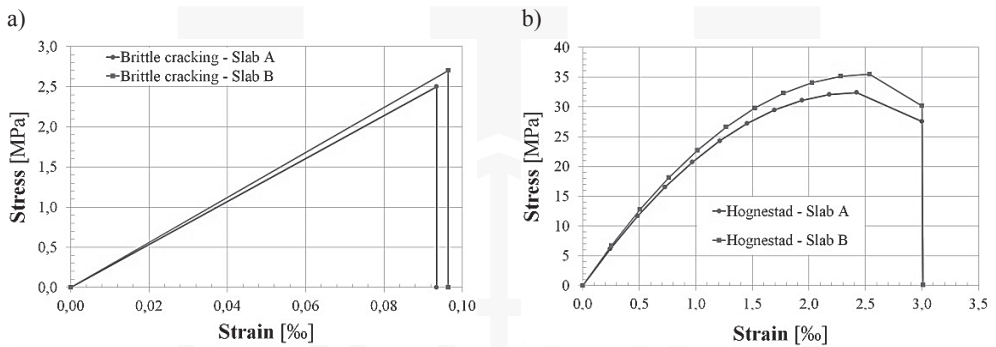


Fig. 3. Assumed models for concrete a) in tension b) in compression

- ‘embedded reinforcement’ was used for reinforcement modeling. With a bond for ordinary reinforcement and without a bond for prestressing reinforcement,
- the strain-stress relationship for ordinary reinforcement was taken after EPSH model presented in report [10] dealing with determining of yield strength. This curve (Fig. 4a) consists of three parts: linear elastic, ideal plastic and material hardening described by parabola eq. (3):

$$f_s = f_u - (f_u - f_y) \cdot \left( \frac{\epsilon_{su} - \epsilon}{\epsilon_{su} - \epsilon_{sh}} \right) \quad (3)$$

- a bilinear stress-strain relationship (linear elastic and material hardening) was used for prestressing reinforcement (Fig. 4b). Assumed 0.1% proof-stress of prestressing steel (yield strength value) equal to 1742 MPa,
- new loading patterns were introduced:
  - 100 and 200 for single-span slabs (A and B respectively) which serve as a comparative members,
  - 111–115 and 211–215 for three-span slab (A and B respectively) which are basic combinations for three-span slab i.e. maximum uniformly distributed loadings act simultaneously in single, both or all spans (Table 5). No partial loading in other spans is allowed.

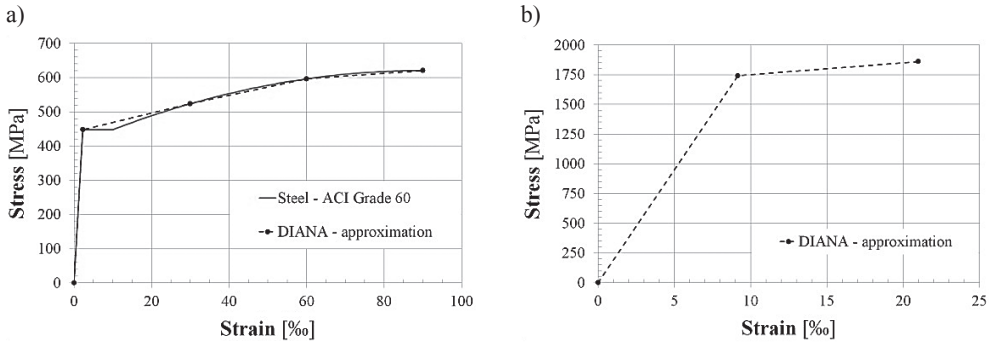


Fig. 4. Assumed models for: a) ordinary reinforcement, b) prestressing wires

Table 4

**Concrete, reinforcement and wires characteristics in numerical analysis**

	Concrete				Ordinary reinforcement			Prestressing reinforcement					
	$f'_c$ [MPa]	$E_{ci}$ [GPa]	$\epsilon_0$ [‰]	$\epsilon_{cu}$ [‰]	$f_{ct}$ [MPa]	$n \times \phi$	$A_s$ [mm <sup>2</sup> ]	$f_y$ [MPa]	$f_u$ [MPa]	$n \times \phi$	$A_p$ [mm <sup>2</sup> ]	$f_{p0.1k}$ [MPa]	$f_{pu}$ [MPa]
Slab A	32.4	26.8	2.42	3.0	2.5	4 #2	127	448	621	4 × 1/4"	127	1742	1860
Slab B	35.5	28.0	2.54	3.0	2.7	7 #2	222			3 × 1/1"	95		

Table 5

**Definition of loading patterns used in numerical analysis**

Span loading according to Fig. 1	Loading pattern – Slab A					Loading pattern – Slab B						
	100	111	112	113	114	115	200	211	212	213	214	215
	–	A	B	A & B	A & C	A, B & C	–	A	B	A & B	A & C	A, B & C

Quadrilateral, 8 nodes plane stress elements were used for meshing (Fig. 5). For each slab 3 different geometrical models were created as shown in Fig. 6:

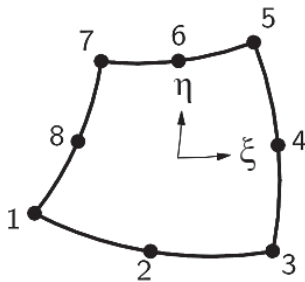


Fig. 5. CQ16M element

- single-span model treated as a comparative member (load patterns 100 and 200),
- three-span model (load patterns 111–114 and 211–215),
- one and semi-span model (left external span and half of internal span – load patterns 115 and 215). This model was created due to problems with achieving convergence for a three-span model in high levels of loading. This was caused by forming 4 plastic hinges – 2 at internal supports and 2 in external spans.

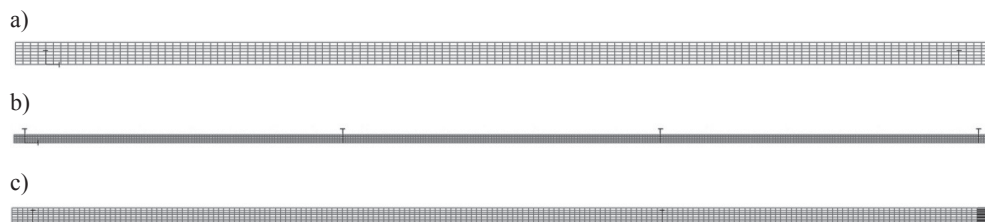


Fig. 6. Meshing for: a) single-span, b) three-span, c) one and semi-span model

#### 4. Numerical analysis – results

Because the majority of considerations about stress increment in unbonded tendons is connected with plastic hinge length, stress values in ordinary reinforcement (bottom  $A_{s1}$  and top  $A_{s2}$ ) are shown in Figures 7–18. Discontinuities visible in these diagrams are connected with a crack pattern. Stresses in reinforcement are greater in cross-sections where cracking occurs and are smaller in those where cracking is not present. Stress values are given in [MPa] and the length of slab (measured from left external support) in [mm].

The most important results from numerical analysis are displayed in Table 6. These are as follows:

- effective prestress  $f_{pe}$ ,
- value of uniformly distributed loading, corresponding stresses  $f_{ps}$  and stress increase  $\Delta f_{ps}$  in unbonded tendons at plasticize of top and bottom reinforcement and at failure,
- maximum values of stresses in the bottom and the top reinforcements ( $\sigma_{s1}$  and  $\sigma_{s2}$ ) and maximum compressive strains in concrete at failure  $\varepsilon_c$ .

Observation of the above charts (Fig. 7–18) and results presented in Table 6 leads to the following conclusions regarding failure mechanism in researched members:

- plastifying of ordinary reinforcement appears earlier in Slab A (combination 100) than in Slab B (combination 200). Such behavior is connected with an ordinary reinforcement ratio which is larger in the second member. Due to the correct crack pattern, the stress increase in unbonded tendons can reach yield strength in both slabs. As a result of the greater value of prestressing reinforcement in first member, it is able to resist larger external loading at failure than the second one,
- the loading of only one external span (combinations 111 and 211) leads to simultaneously plastifying of ordinary reinforcement in the loaded span and internal support. Due to the same reasons as above plastifying of ordinary steel occurs earlier in Slab A than Slab B. Load increase results in failure of the member at internal support caused by the crushing of concrete. Behaviour which is different to that which is described above can be observed. Larger value of ordinary reinforcement ratio in the second member has positive influence on plastic hinge formation both at internal support and external reinforcement. It should be highlighted that in both cases, the stress increment in unbonded tendons is lower than the yield strength of ordinary reinforcement and is greater for Slab B. These two facts decide that this member could resist greater external loading,

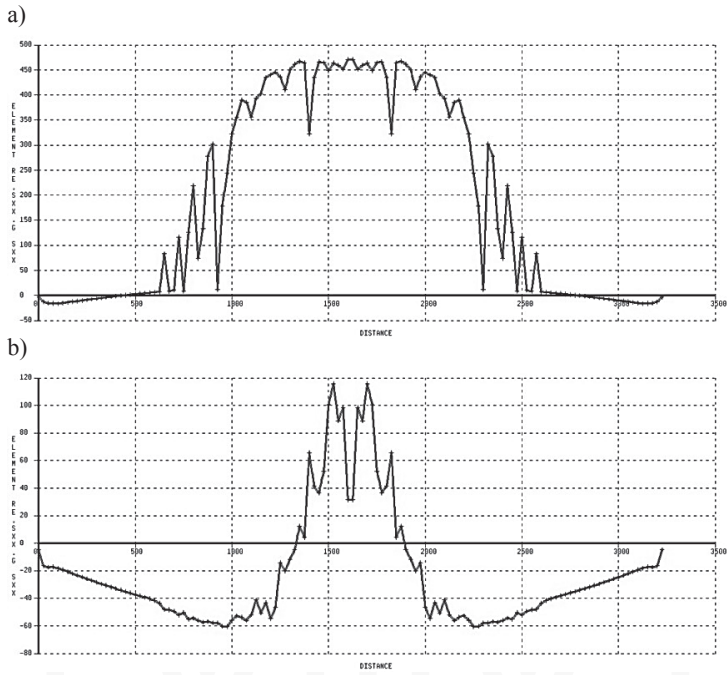


Fig. 7. Stresses in ordinary reinforcement in single-span model (100): a) bottom, b) top

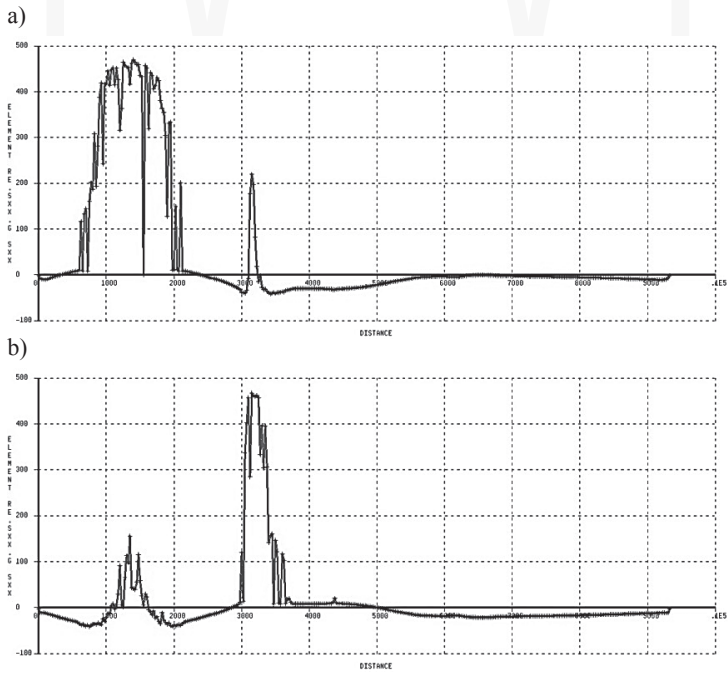


Fig. 8. Stresses in ordinary reinforcement in three-span model (111): a) bottom, b) top

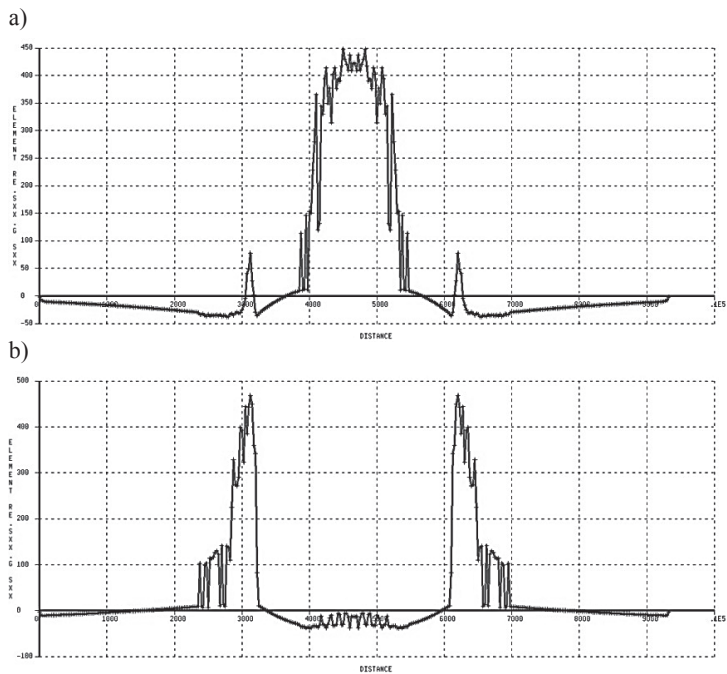


Fig. 9. Stresses in ordinary reinforcement in three-span model (112): a) bottom, b) top

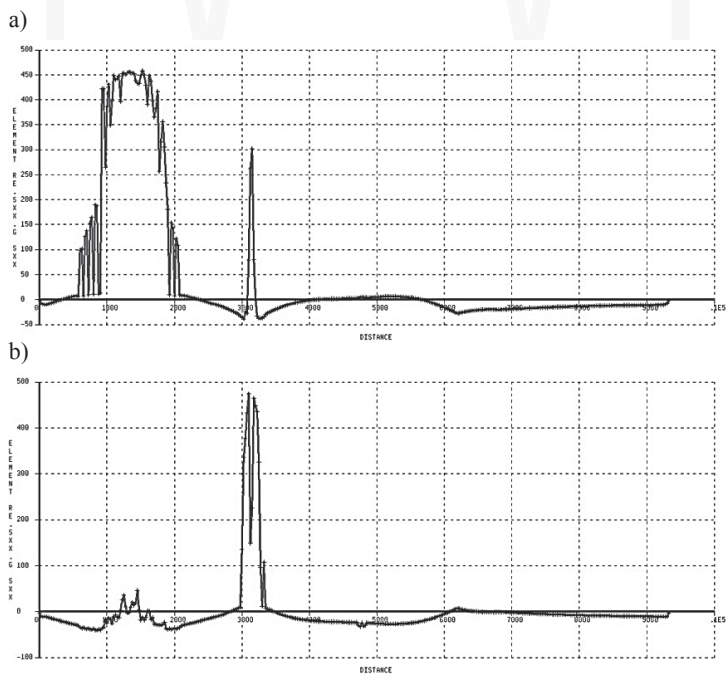


Fig. 10. Stresses in ordinary reinforcement in three-span model (113): a) bottom, b) top

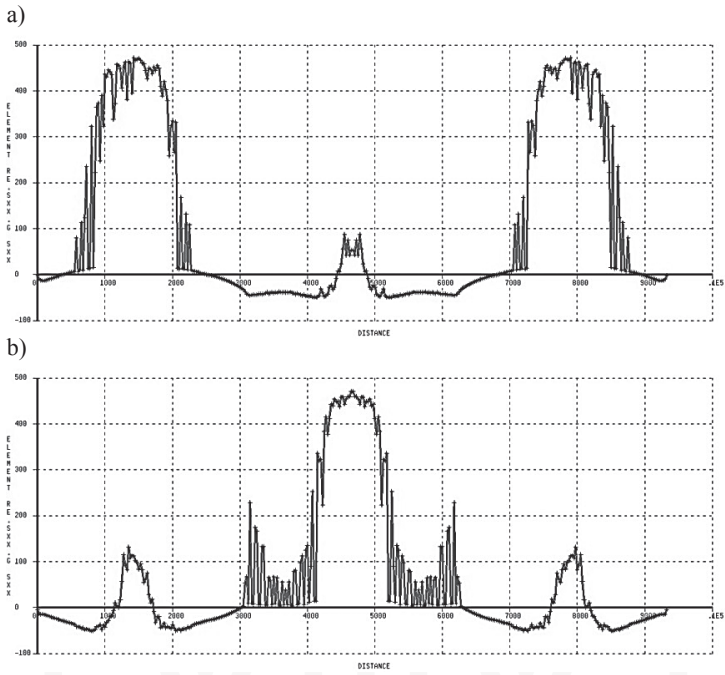


Fig. 11. Stresses in ordinary reinforcement in three-span model (114): a) bottom, b) top

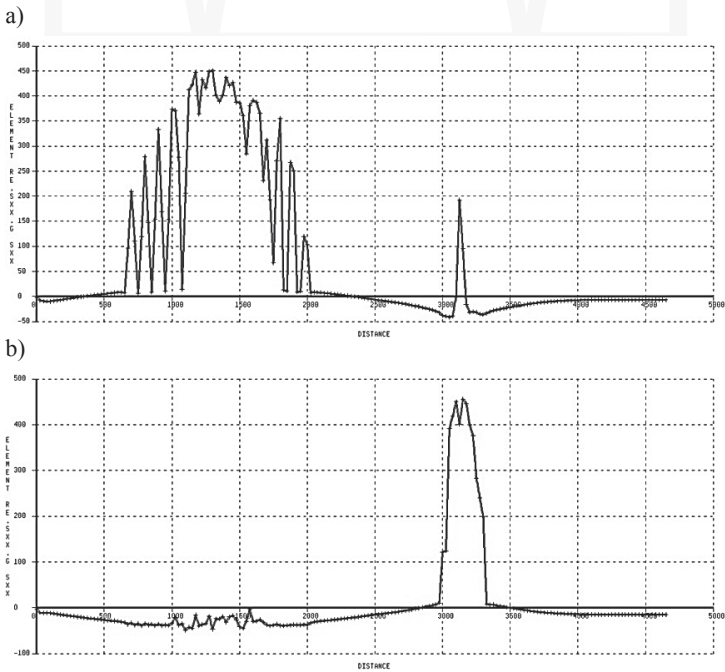


Fig. 12. Stresses in ordinary reinforcement in one and semi-span model (115): a) bottom, b) top

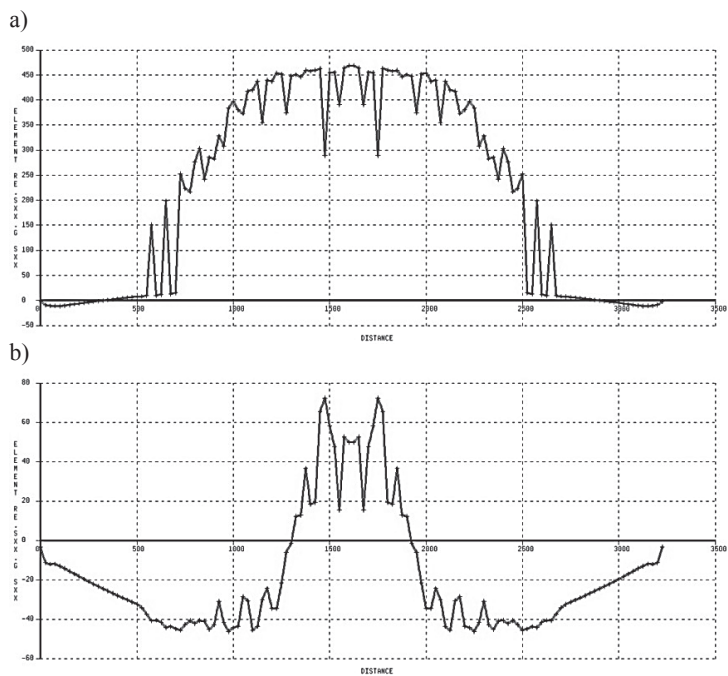


Fig. 13. Stresses in ordinary reinforcement in single-span model (200): a) bottom, b) top

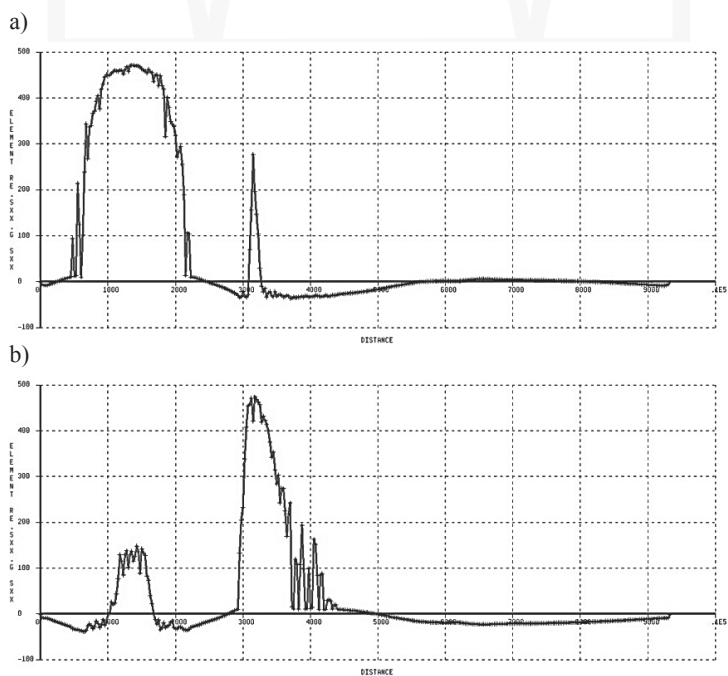


Fig. 14. Stresses in ordinary reinforcement in three-span model (211): a) bottom, b) top

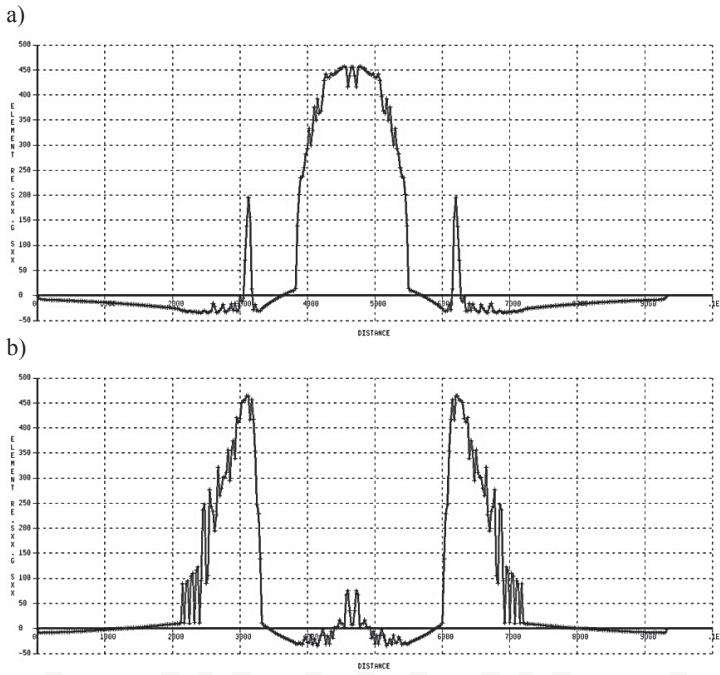


Fig. 15. Stresses in ordinary reinforcement in three-span model (212): a) bottom, b) top

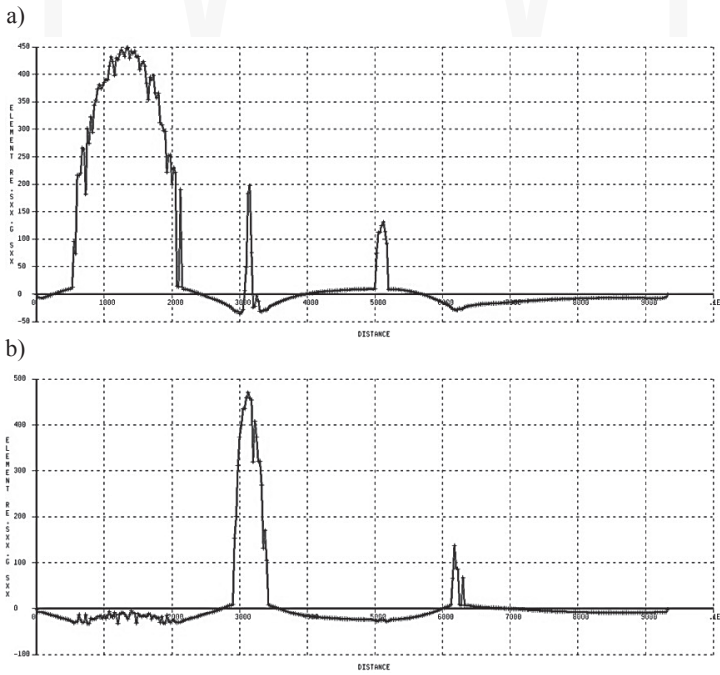


Fig. 16. Stresses in ordinary reinforcement in three-span model (213): a) bottom, b) top

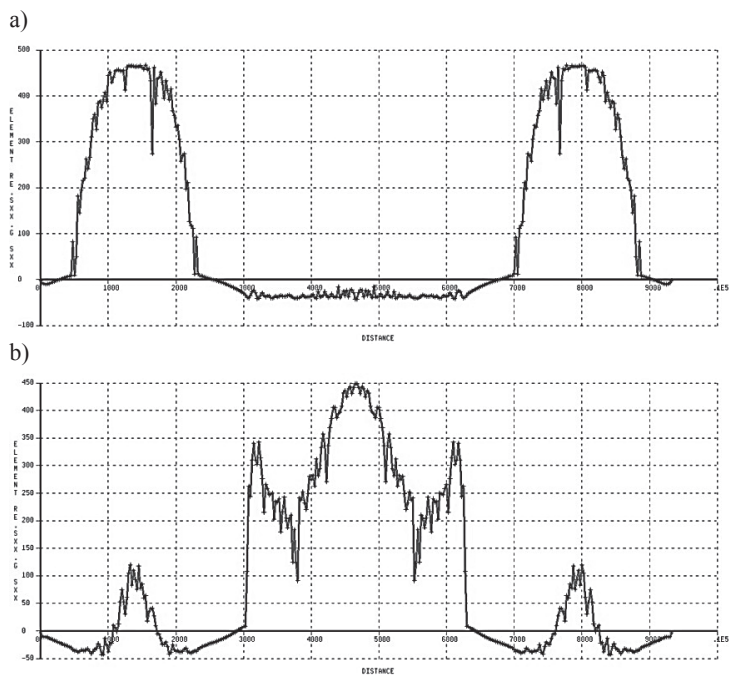


Fig. 17. Stresses in ordinary reinforcement in three-span model (214): a) bottom, b) top

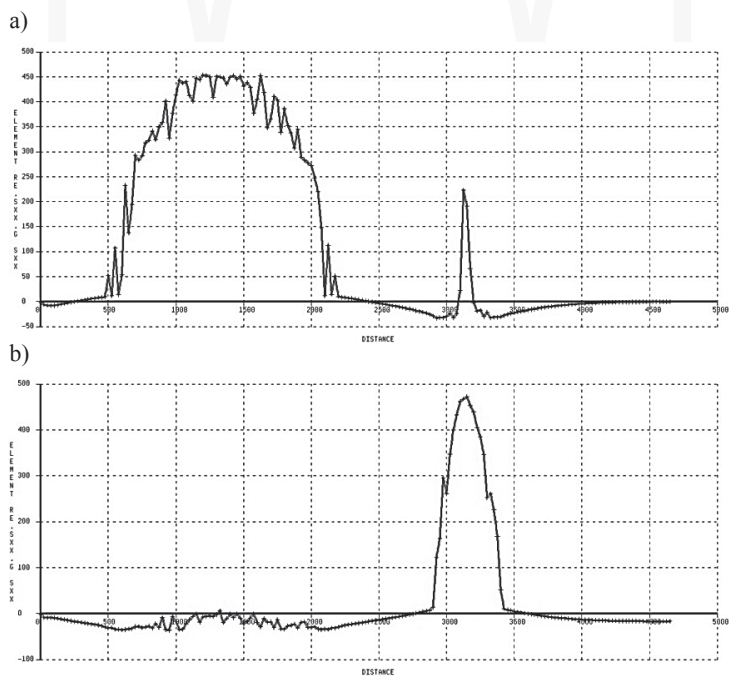


Fig. 18. Stresses in ordinary reinforcement in one and semi-span model (215): a) bottom, b) top

Numerical analysis results for different loading patterns

		Loading pattern – Slab A						Loading pattern – Slab B					
		100	111	112	113	114	115	200	211	212	213	214	215
$f_{pe}$ [MPa]		968	968	968	968	968	968	1006	1006	1006	1006	1006	1006
Plasticize $A_{s(top)}$ [kN/m]		–	7.7	11.6	6.6	8.9	6.9	–	8.6	13.5	6.8	11.7	7.9
$f_{ps}$ [MPa]		–	1032	1025	998	1212	1031	–	1092	1105	1054	1549	1117
$\Delta f_{ps}$ [MPa]		–	64	57	30	244	63	–	86	99	48	543	111
Plasticize $A_{s(bottom)}$ [kN/m]		4.3	7.7	13.2	7.6	7.7	8.4	5.2	8.6	14.3	9.0	8.4	9.6
$f_{ps}$ [MPa]		1160	1032	1071	1031	1110	1102	1285	1092	1123	1104	1186	1202
$\Delta f_{ps}$ [MPa]		192	64	103	63	142	134	279	86	117	98	180	196
Failure [kN/m]		8.4	9.3	13.2	8.8	10.9	8.4	7.7	11.3	16.0	9.1	11.7	10.4
$f_{ps}$ [MPa]		1742	1139	1071	1080	1477	1102	1731	1310	1209	1107	1549	1252
$\Delta f_{ps}$ [MPa]		774	171	103	112	509	134	725	304	203	101	543	246
Support 2 or Span B	$\sigma_{s1}$ [MPa]	–	467	468	474	471	456	–	474	464	470	449	472
	$\sigma_{s2}$ [MPa]	–	219	78	300	87	192	–	276	195	200	–16	225
	$\varepsilon_c$ [‰]	–	–3.07	–1.52	–4.17	–1.77	–2.88	–	–3.64	–2.95	–2.97	–0.98	–3.68
Span	$\sigma_{s1}$ [MPa]	471	470	448	458	472	451	469	471	457	449	467	453
	$\sigma_{s2}$ [MPa]	116	155	–39	45	132	–3	72	148	75	–33	120	6
	$\varepsilon_c$ [‰]	–2.32	–1.68	–0.95	–1.24	–2.07	–1.86	–2.01	–2.25	–1.60	–0.89	–1.99	–1.16

- for loading combinations where the internal span was loaded (112, 113, 115, 212, 213 and 215) plastifying of ordinary reinforcement appears earlier at supports than in spans. Due to the same reasons as above plastifying of ordinary steel occurs earlier in Slab A than Slab B. Similar behaviour as described above can be observed for combinations 111 and 211 – greater stress increment in unbonded tendons and accompanying resistance. This phenomenon is different in combinations where only the internal span is loaded (113 and 213). A slightly greater stress increment was achieved in Slab A, but it has no influence on the bending resistance of these two members. It should be underlined that only in loading combination 112 value of compressive strains at internal support was far from ultimate strain for concrete (3‰). In other cases, a further increase of loading will lead not only to exceeding the limit value of strains in tensile reinforcement  $A_{s1}$  (10‰) but also will cause crushing of the concrete,

- simultaneously loading of external spans (combinations 114 and 214) leads to earlier plastifying in spans. Instead of forming two plastic hinges at internal supports plastifying of top reinforcement in internal span could be observed. Such behaviour is caused by a lack of loading in this span and an additional action which comes from prestress. Similarly like previously greater value of ordinary reinforcement ratio leads to achieving larger values of stress increase in unbonded tendons. Also, bending resistance of Slab B is greater. Concrete strains at ultimate at support cross-section are very close to 2‰.

The stress increment value is related to the effort of spans' cross-sections (where long plastic hinges are formed) and effort of supports' cross-sections (where short plastic hinges are formed). If plastifying of ordinary reinforcement appears earlier in spans greater value of stress increment in unbonded tendons should be expected. The following conclusion can be drawn from results comparison of combinations where only external span is loaded (111 and 211) and other combinations where additional loading is acting in internal span (113, 213, 115 and 215). It has negative influence on stress increment in unbonded tendons because it leads to faster member failure at support and limits possibility of forming long plastic hinge in spans. Comparison of loading single external span (111 and 211) and internal span (112 and 212) enables to observe influence of which span is loaded. First loading pattern makes possible to form long plastic hinge in span which leads to greater stress increment in unbonded tendons. Greatest values of stress increment in unbonded tendons were achieved on case of simultaneously loading of external spans (114 and 214). It is worth to emphasize that they were not so big as for single-span members (100 and 200). Stress increase in unbonded tendons is not only influenced by pattern loading but also by ordinary reinforcement ratio which enables proper formation of plastic hinges (especially at support cross-sections). Its influence could be observed also in above numerical analysis. Of course it could be questionable due to different concrete properties used for Slab A and Slab B. Without doubt it should be claimed that 10% difference in compressive strength will not cause almost two times higher stress increase in unbonded tendons in some cases.

## 5. Loading pattern as a parameter

The consideration of the loading pattern as a parameter was taken by a few researchers. Naaman [4] presents this in a very simple way as the ratio of loaded spans to total spans length (distance between anchorages). In one of his first papers [5] Harajli proposes to express it in a very similar way as the ratio of the number of loaded spans to the total number of spans. Assuming equal length of all spans leads to the same value of loading patterns expressed by the equation below (4). For simply supported member value of this parameter is equal to 1.

$$\frac{L_1}{L_2} = \frac{n_o}{n} \quad (4)$$

In a subsequent paper [6], Harajli connected the value of this parameter with the number and length of plastic hinges formed at ultimate eq. (5). Plastic hinge length  $L_0$  is influenced by the type of acting loading (uniformly distributed loading, one-point or two-point loading) and the manner of determining number of plastic hinges is presented in Fig. 19.

$$\frac{n_p}{n} \tag{5}$$

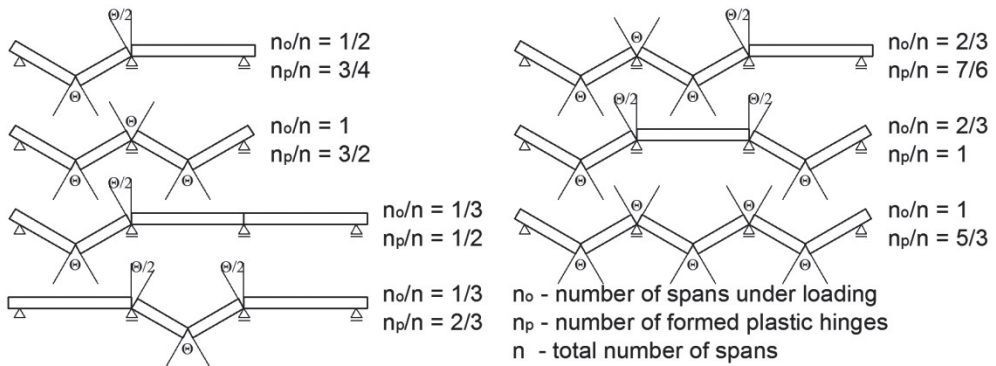


Fig. 19. Load pattern factor values – two- and three-span members

Some discrepancies could be found in abovementioned theory. Factor  $f$  which depends on the loading type, expresses only one plastic hinge length. It should be added that plastic hinge length differs in span where different types of loading could be acting ( $f = 3, 6$  or  $\infty$ ) and at support where reaction should be rather associated with one-point loading ( $f = \infty$ ).

The next paper [7] deals with these doubts by introducing the distinction between plastic hinges formed in spans  $n_p^+$  and at supports  $n_p^-$ . Both of these are connected and expressed by  $N_p$  factor. The method of calculating the  $N_p$  factor is presented in Figure 20. The number of plastic hinges in spans  $n_p^+$  and at supports  $n_p^-$  are presented. Moreover two values of this factor which depend on type of loading are presented for one-point loading (1P) and uniformly distributed loading ( $q$ ) respectively. It is worth emphasising that this value for simply supported beams equals 10.5 and 14 accordingly.

The load pattern parameter is expressed in equation (6) as a ratio of  $N_p$  value divided by total member length  $L$  to  $N_{p(1span)}$  value calculated for single-span member divided by length  $L_{(1span)}$  of span.

$$\frac{N_p / L}{N_{p(1span)} / L_{(1span)}} \tag{6}$$

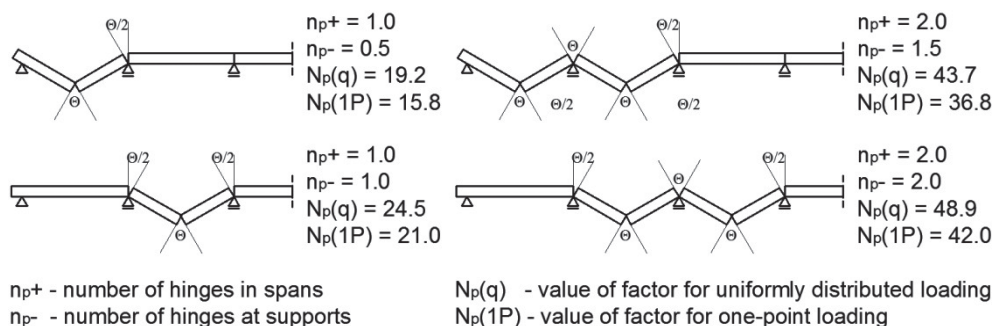


Fig. 20. Load pattern factor calculation with span and support hinge distinction taken into account

The following conclusions can be drawn from this short overview of the load pattern parameter and its influence on the stress increase in unbonded tendons:

- the first approach (eq. 4) treats this problem in a simplified way. The failure mechanism which has an influence on stress increment in unbonded tendons is not taken into consideration. It makes no significance whether or not external or internal span is loaded. The loading of all spans simultaneously should lead to the same value of stress increase in unbonded tendons as in simply supported members,
- the second approach (eq. 5) takes the failure mechanism into consideration and the stress increment in unbonded tendons is dependent on the number and length of plastic hinges. Their lengths are connected with the type of acting loading. However, the fact that plastic hinge lengths are smaller at supports is not taken into account. Support reactions should be treated in a similar way as point loading. In case of all or almost all spans loaded load pattern value could be greater than 1. This indicates that stress increase in unbonded tendons could be greater than in comparative simply supported members,
- the third approach (eq. 6) introduces an amendment considering plastic hinge length at supports. Once again, there is the possibility to achieve greater values of the stress increment in unbonded tendons in comparison to simply supported members.

Table 7 contains values of the load pattern factor calculated in accordance with the above equations (4)–(6) compared to the results of numerical calculations. It could be observed that in the case of loading acting in 2 or 3 spans, values of stress increment in unbonded tendons could be as large or even greater than calculated for simply supported members. Results gained from numerical analysis contradict these outcomes. It has been proven that there are correlations between the number and the length of plastic hinges created at ultimate; moreover they indicate the importance of a plastic hinge formation sequence. The greatest stress increase in unbonded tendons has been obtained for simultaneously loading acting in both external spans. In this case plastifying of ordinary reinforcement occurs firstly in spans which enables the formation of long plastic hinges. Gained values of stress increase in unbonded tendons do not exceed 75% of values achieved for simply supported members. In other cases short plastic hinges were formed at supports and as a consequence low stress increase in prestressing steel was obtained. Its value was within the limit <13÷42> percent of the value received for simply supported members. It should be mentioned that increasing  $q_s$  factor compared to  $q_e$  factor does not lead to a lower stress increment in prestressing

steel despite the fact that such behaviour was observed in both experimental and theoretical research on simply supported members – on the contrary its increase was triggered. This could be explained by improved behaviour at support cross-sections and better redistribution of bending moments.

Table 7

**Load patterns values – comparison of theoretical approaches and numerical results**

	Loading pattern – Slab A						Loading pattern – Slab B					
Load combination	100	111	112	113	114	115	200	211	212	213	214	215
Parameter value (4)	1	1/3	1/3	2/3	2/3	1	1	1/3	1/3	2/3	2/3	1
Parameter value (5)	1	1/2	2/3	7/6	1	5/3	1	1/2	2/3	7/6	1	5/3
Parameter value (6)	14.0	19.2	24.5	43.7	38.4	62.9	14.0	19.2	24.5	43.7	38.4	62.9
$N_p/N_{p(1\text{ span})}$	100%	46%	58%	104%	92%	150%	100%	46%	58%	104%	92%	150%
$\Delta f_{ps}$ [MPa] – DIANA	774	171	103	112	509	134	725	304	203	101	543	246
$\Delta f_{ps} \Delta f_{ps(1\text{ span})}$	100%	22%	13%	14%	66%	17%	100%	42%	28%	14%	75%	34%

It can be assumed that the last proposal of Harajli introducing the load pattern factor as a function of the number and the length of plastic hinges could be true but only in specific conditions. The following assumptions and limitations regarding the formation of plastic hinges are introduced by the author:

- all plastic hinges behave similarly i.e. the concrete compressive block depth  $c$ , depth and area of prestressing reinforcement  $d_{ps}$  and  $A_{ps}$  and ordinary reinforcement  $d_s$  and  $A_s$  are the same or very similar in all span and support cross-sections,
- the section is rectangular or has the rectangular section behaviour,
- stress increase at ultimate above the effective prestress  $\Delta f_{ps}$  is assumed to be not greater than  $(0.95f_{py} - f_{se})$  which assures that the stress in tendons will not reach the yield strength of prestressing reinforcement.

According to the author of this paper, similar behaviour of all plastic hinges could be assured by simultaneous plastifying of ordinary reinforcement by the means below:

- bending moment equalisation in critical cross-sections,
  - span bending moments – changing multi-span member geometry, e.g. reducing lengths of the external span in comparison to internal spans,
  - support bending moments – tendon duct adjustment allowing unloading of internal supports,
- adding ordinary reinforcement at internal supports and external spans.

These treatments cannot be implemented for all possible load combinations due to the fact that the ratio of bending moments at the support and span will change and will be different for e.g. combination 113 and 114. It is recommended to arrange reinforcing bars in such a way that ordinary reinforcement will plasticise firstly in spans and then at supports. This

allows forming longer plastic hinges and benefitting from greater stress increase in unbonded tendons. However, the possibility to obtain stress increase in unbonded tendons in multi-span members at the same level as for simply supported members is doubtful.

It should be underlined that during the design process of multi-span members bending moment resistance of support and span cross-sections is calculated with usage of loading patterns giving maximum values of moments at crucial cross-sections. In prestressed structures post-tensioned with unbonded tendons, additional span loading (combinations 114 and 214) in comparison with single-span loading (combinations 111 and 211), could bring more advantages (greater stress increase in prestressing steel) than disadvantages (slightly greater bending moment). In the case of structures with a higher number of spans this phenomenon can also be observed during the dimensioning of support cross-section. Ultimate Limit State will not be reached by sophisticated loading pattern but for simple scheme where one, external span is loaded.

## 6. Final conclusions

The design process of multi-span structures post-tensioned with unbonded tendons can differ from that used for reinforced concrete, pretensioned and members post-tensioned with bonded tendons. It may appear that ULS is reached by different load patterns to which we got used to. Theoretical approaches proposed by various authors should be applied with caution. The possibility to achieve such a great stress increase as that found in simply supported members is questionable. Extending the bending resistance of the whole structure is connected with enabling the formation of long plastic hinges in spans via the arrangement of additional reinforcement at supports which assures the proper redistribution of bending moments.

## References

- [1] Building Code Requirements for Structural Concrete (ACI 318M-14).
- [2] PN-EN 1992-1-1:2004 Eurokod 2: Projektowanie konstrukcji z betonu – Część 1: Reguły ogólne i reguły dla budynków.
- [3] PN-B-03264:2002 Konstrukcje betonowe, żelbetowe i sprężone. Obliczenia statyczne i projektowanie.
- [4] Naaman A., Alkhairi F., *Stress at Ultimate in Unbonded Post-Tensioning Tendons: Part II - Proposed Methodology*, ACI Structural Journal, Vol. 88, No. 6, 1991, 683–692.
- [5] Harajli M., Hijazi S., *Evaluation of the Ultimate Steel Stress in Partially Prestressed Concrete Members*, PCI Journal, Vol. 36 No. 1 1991, 62–82.
- [6] Harajli M., *On the Stress in Unbonded Tendons at Ultimate: Critical Assessment and Proposed Changes*, ACI Structural Journal, Vol. 103, No. 6, 2006, 803–812.

- [7] Harajli M., *Tendon Stress at Ultimate in Continuous Unbonded Post-Tensioned Members: Proposed Modification of ACI 318, Eq. (18-4) and (18-5)*, ACI Structural Journal, Vol. 109, No. 2, 2012, 183–192.
- [8] Burns N.H., Charney F.A., Vines W.R., *Tests of One Way Slabs with Unbonded Tendons*, PCI Journal, Vol. 23, No. 5, October 1978, 66–83.
- [9] DIANA, *User's manual: Finite element analysis*, TNO DIANA, Delft.
- [10] CHARLES PANKOW FOUNDATION RGA 04-13, *Determination of Yield Strength for Nonprestressed Steel Reinforcement*, Final Report December 31, 2013, WJE No. 2013.4171.

